https://doi.org/10.1595/205651323X16648726195503 *Johnson Matthey Technol. Rev.*, 2023, **67**, (3), 249–265

JOHNSON MATTHEY
TECHNOLOGY REVIEW
technology.matthey.com

Advanced Supports for Noble Metal Catalysts in Proton Exchange Membrane Water Electrolysers: A Review

Improving the performance, stability, durability and cost of iridium- and platinum-based catalytic materials

Pere L. Cabot*
Laboratory of Electrochemistry of Materials and the Environment, Department of Materials Science and Physical Chemistry, Faculty of Chemistry, University of Barcelona, Martí and Franquès 1, 08028 Barcelona, Spain

María V. Martínez-Huerta
Institute of Catalysis and Petrochemistry, Spanish Council for Scientific Research (CSIC), C/ Marie Curie, 2. Cantoblanco, 28049 Madrid, Spain

Francisco Alcaide
Laboratory of Electrochemistry of Materials and the Environment, Department of Materials Science and Physical Chemistry, Faculty of Chemistry, University of Barcelona, Martí and Franquès 1, 08028 Barcelona, Spain; CIDETEC, Basque Research and Technology Alliance (BRTA), Paseo Miramón, 196, 20014 San Sebastián, Spain

***Email:** p.cabot@ub.edu

PEER REVIEWED

Received 29th July 2020; Revised 21st September 2022; Accepted 3rd October 2022; Online 4th October 2022

Renewable and low-carbon hydrogen will contribute to a future climate-neutral economy as a fuel, clean energy carrier and feedstock. One of the main concerns when considering its production by the present proton exchange membrane water electrolysers (PEMWE) is the use of scarce and expensive noble metals as catalysts for the hydrogen evolution reaction (HER) and oxygen evolution reaction (OER), because they contribute to increase the cost of the technology. Several strategies have been developed to overcome this drawback, such as optimising the catalyst loading in the electrodes and alloying or using alternative catalyst supports, always with the aim to maintain or even increase electrolyser performance and durability. In this review, we examine the latest developments in HER and OER catalysts intended for practical PEMWE systems, which point in the short term to the use of platinum and iridium nanoparticles highly dispersed at low loadings on conductive non-carbon supports.

1. Introduction

Renewable energy sources have gained significant attention due to the limited amounts of fossil fuels and their environmental impact. The increasing release of carbon dioxide, nitrogen oxides, heavy metals, ashes, tars and organic compounds from the combustion of fossil fuels to meet global energy demand has led to a rapid increase in pollutants and greenhouse gases in the air (1, 2). Today, concerns about air pollution and climate change drive the search for environmentally friendly, accessible and economically attractive renewable energy sources as alternatives to fossil fuels.

Hydrogen is the 'clean fuel of the future' because water is the only product expected (although residual pollutants can appear depending on the

purity of the fuel and the oxidiser). Pure hydrogen allows clean energy to be obtained (3). However, it is not directly available for use in nature and therefore, it has to be produced (4). The current annual production of hydrogen is about 0.1 billion tonnes, the most part being used for petroleum and metals refining (47%) and ammonia production (45%). A small fraction is applied for electronics fabrication, the food industry and as fuel for transportation (5).

Nikolaidis and Poullikkas (4) have summarised the main advantages and disadvantages of the different methods of hydrogen production. Steam reforming of hydrocarbons is the most developed method, with existing infrastructure and efficiencies in the range 74–85%. Partial oxidation and autothermal steam reforming of hydrocarbons are proven technologies with smaller efficiencies in the range 60–75%. All these methods produce CO_2 as byproduct, depending on the fossil fuel. There are alternative methods using raw materials coming from renewable technologies, namely biomass and water. The pyrolysis of biomass presents efficiencies of 35–50% and is CO_2-neutral, but its main disadvantages are tar formation and the variable hydrogen content depending on the seasonal availability and impurities of the feedstock. The dark fermentation of biomass also has good efficiencies in the range 60–80% and is CO_2-neutral, but its major disadvantages are the formation of fatty acids, which are organic pollutants that should be removed, low hydrogen production rates, low yields and the need for large reactor volumes.

Production methods utilising water as the only raw material produce hydrogen through water splitting processes such as electrolysis, thermolysis and photoelectrolysis. Thermolysis of water, with efficiencies in the range 20–45%, is clean and sustainable with oxygen being the only byproduct, but its major disadvantages are the toxicity of the elements used, corrosion problems and the need for high capital investment. Photoelectrolysis of water is also interesting since it is free from emissions and oxygen is the only byproduct, but it requires sunlight, has efficiencies of about 0.06% and suitable photocatalytic materials are needed. Conversely, electrolysis is a proven technology, with existing infrastructures and good efficiencies in the range 40–60%, with only oxygen as byproduct. Although a high capital investment is required and hydrogen produced by this method is still more expensive than that obtained from hydrocarbon reforming, water electrolysis appears to be an environmentally friendly hydrogen generation process and will be a key technique in the hydrogen economy.

Electrolysis is already a basic technique to provide hydrogen in small quantities for applications such as the food and semiconductor industries (5). Despite this, water electrolysis only contributes about 4% of overall hydrogen production in the world today (5). This may significantly change in the next few decades since solar and wind renewable energy resources are expected to increase, replacing fossil fuels for environmental reasons. If energy production by these methods exceeds the electricity demand, energy storage as hydrogen fuel can be a potential solution (1). This is particularly interesting because renewable resources are intermittent and therefore excess energy in operation can be used in water electrolysis for hydrogen production.

Alkaline electrolysis is the oldest and most mature technique. It uses a thin ceramic porous diaphragm submerged in a liquid alkaline electrolyte (6–8). It is also possible to use anion exchange membrane technology in alkaline water electrolysis. However, this is a long way from commercialisation. In the meantime, water electrolysis using PEMWEs is a recent and very attractive technique from an industrial viewpoint because the PEMWE is a compact device of simple construction and flexible dynamic operation in which a proton exchange membrane (PEM) replaces the liquid electrolyte (9). **Figure 1** shows a schematic of a single cell of a PEMWE (10). The PEM is an acidic solid polymer electrolyte with very good proton conductivity (solid polymer electrolyte in **Figure 1**). Perfluorinated sulfonic-acid (PFSA) PEM membranes such as Nafion® are commonly used (11). The anode and cathode reactions for water electrolysis in acidic media are given by Equations (i) and (ii) for the OER and HER, respectively (3):

$$H_2O \rightarrow ½\ O_2 + 2\ H^+ + 2\ e^- \quad (i)$$

$$2\ H^+ + 2\ e^- \rightarrow H_2 \quad (ii)$$

The standard (reduction) electrode potentials are 1.23 V and 0.00 V *vs*. standard hydrogen electrode, respectively, therefore the standard Gibbs energy of the overall Equation (iii) (given by the summation of Equations (i) and (ii)):

$$H_2O \rightarrow ½\ O_2 + H_2 \quad (iii)$$

is $\Delta G^o = -2 \times 96{,}486\ C\ mol_{H2O}^{-1} \times (-1.23\ V) = 2.37 \times 10^5\ J\ mol_{H2O}^{-1} > 0$, meaning that this process

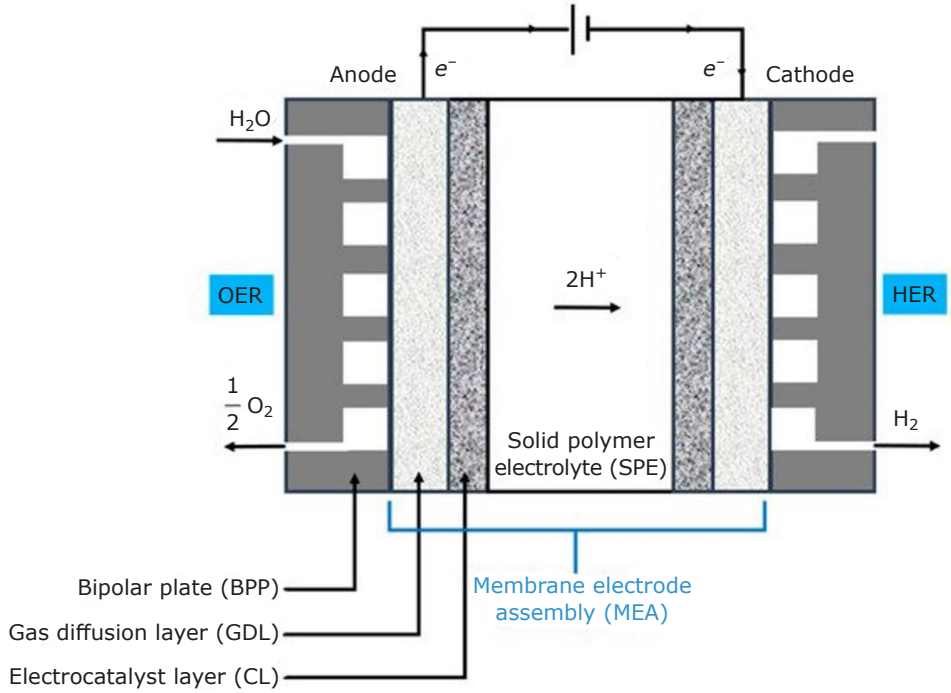

Fig. 1. Scheme of a single cell of a PEMWE. Reproduced from (10) under a Creative Commons CC BY license

requires energy, which can be provided by a power source moving electrons from the anode to the cathode terminals. As shown in **Figure 1**, water is introduced in liquid or vapour form, depending on the temperature, in the anode compartment where Equation (i) takes place. The protons produced through Equation (i) are transported by the electric field through the PEM to the cathode, where they are reduced according to Equation (ii). The acidic solution is retained in the membrane, thus reducing corrosion problems. The PEM must be thin to reduce the ohmic drop, which reduces the voltage needed for water electrolysis. In addition, it is not an electron conductor and behaves as a separator between the anode and the cathode, thus avoiding internal short-circuits. Moreover, it presents good chemical, mechanical and dimensional stability, with low permeability to hydrogen and oxygen. The anode and the cathode catalyst layers or electrocatalyst layers (CLs in **Figure 1**) are placed on each side of the PEM. The gas diffusion layers allow diffusion of reactants through them. The set integrated by the PEM and CLs is known as the membrane electrode assembly (MEA). Note also that the reactants circulate through the gas channels of the bipolar plates (BPPs in **Figure 1**), which allow the complete stack to be built up by means of the electrical connection between the cathode and the anode of adjacent cells.

Although PFSAs suffer dehydration over 100°C (11) and there is a consequent thermal limit in its practical use, the PEM offers additional advantages to the liquid alkaline electrolyte: (a) there are no anionic concentration gradients (as the anionic charges are fixed, fewer species are transported and the complexity of the system is reduced); (b) the gases are evolved at the back of the electrodes and do not contribute to the internal cell resistance, which is mainly due to the PEM (5); and (c) they are free from carbonate formation problems, thus providing highly compressed and pure hydrogen with high efficiency (1).

However, unlike alkaline electrolytes, acidic electrolytes require corrosion-resistant noble metals as electrocatalysts (12). The main components affecting performance and durability of PEMWE stacks are MEAs, in which at present iridium is the electrocatalyst for the OER and platinum for the HER (13–16). Current densities in the range 0.6–2.0 A cm^{-2} for applied single cell voltages between 1.8–2.2 V can now be obtained (17). PEMWEs are in the early market introduction phase in the energy sector and the focus is on their durability and reliability rather on their cost (13). A recent estimate is that MEAs represent about 19% of the overall stack cost (18). The PEM itself plays a role because it contributes a significant ohmic loss, increasing with thickness, and must ensure robustness and low hydrogen and oxygen crossover. Nafion® 115 and 117, 120–200 µm in thickness are currently used, typically contributing about 5% of the cost of the PEMWE stack, but there is the possibility of introducing nanoparticles (NPs) or nanofibres in thinner PEMs with lower ionic resistance resulting

in good mechanical stability and low oxygen and hydrogen crossover (14, 15, 19–22).

The MEA is normally fabricated by directly depositing the electrocatalysts onto the PEM or by transferring them onto the PEM by a decal process (23). This latter procedure is known as the catalyst coating membrane approach (24, 25). The OER presents a more sluggish kinetics than the HER, therefore it significantly contributes to the overall polarisation. Iridium metal and IrO_2 are the present state-of-the-art OER catalyst in PEMWEs (12, 14), providing a suitable balance between activity and stability and representing about 8% of the stack cost. With a typical loading of 2 mg_{Ir} cm^{-2} (23), an amount of about 500 kg of iridium is needed for a gigawatt-plant working at 4 W cm^{-2} (14). This is a large amount of iridium considering the annual worldwide production of about 9000 kg $year^{-1}$ (2). Therefore, there is a need to reduce the iridium loading while improving the OER performance. The catalyst for the HER is platinum with a loading of about 0.3–0.5 mg cm^{-2} (12, 20, 26), contributing about 6% of the MEA cost, although it has been pointed out that this could be significantly reduced without performance loss (25). Other important components of PEMWEs are the bipolar plates and the porous transport layers, which contribute about 68–74% of the overall stack cost. The cell and stack balances account for the remaining percentage (14, 18).

PEMWEs use noble metals because of the advantages mentioned above. After intensive research, new components based on non-noble metals may be possible in the long-term, but in the short-term, there is still room to achieve better performance, durability and cost reduction with iridium and platinum (14). It is estimated that the overall cost could be reduced by about half by using advanced manufacturing techniques, especially for flow fields and separators (18). The catalytic material and catalyst loading are also crucial to obtain suitable performance, durability and cost (14). A good strategy to decrease catalyst cost may be to improve the stability of the support, enabling better dispersion to increase their utilisation.

Feng *et al*. (21) have summarised the degradation mechanisms of PEMWE components. The main problems with the electrocatalysts were dissolution, deactivation and agglomeration together with support passivation which would impede the current flow. This points to promising solutions such as addition of inert oxides, the use of binary or ternary solid-solution catalysts or tailoring the morphology of the catalyst. Recent PEMWE degradation studies suggested that the measured cell voltage increase was mainly due to reversible changes in the oxidation state of the iridium-based catalyst and that the real degradation took place in the ohmic and mass transport overpotential region at high current densities and long-time operation (13).

In this review, recent approaches to improve performance, stability, durability and cost of iridium- and platinum-based catalytic materials in current use are examined as specific objectives in the short-term development of PEMWEs. Attention is paid to catalyst loading and dispersion onto different supports, especially non-carbonaceous ones, which are particularly important in the anode of the PEMWEs due to the oxidative nature of this environment.

2. Supported Catalysts for the Hydrogen Evolution Reaction

As mentioned in the previous section, the most effective electrocatalysts for the HER in practical PEMWE are those based on platinum. However, the high cost and scarcity of platinum are a drawback in the development of PEMWE for large-scale applications. Reducing the amount of platinum is the main strategy to decrease the cathode cost contribution to PEMWEs (25, 27–30). Platinum black has been employed in the cathode of PEMWEs (30), but the platinum loading can be reduced by improving the catalyst dispersion on high specific surface area supports based on carbon or non-carbon materials. A further strategy involves the development of platinum-based alloys.

2.1 Platinum-Based Catalysts Supported on Carbon Materials

It is generally accepted that highly dispersed platinum-on-carbon is the benchmark HER catalyst for PEMWEs, the carbon black Vulcan® XC-72 being the most common (15, 19, 22, 23, 25, 26, 29, 31, 32). Carbon-based materials are widely used as electrocatalyst supports because of their large surface area, high electron conductivity and stability. A PEMWE single cell based on Nafion® NR117 containing 0.4 mg_{Pt} cm^{-2} (40 wt% platinum supported on Vulcan® XC-72) and 2.5 mg cm^{-2} of IrO_2 was reported (32) and it showed 1.7 V at 1 A cm^{-2} and 90°C. The average voltage degradation rate was *ca*. 35.5 μV h^{-1} after 4000 h at these experimental conditions.

Other materials like graphitic nanofibers (GNF) have been proposed as catalyst supports because their textural properties can favour the transport of gases. In particular, the performance of GNF-supported catalysts was found to be better than that of catalysts supported on Vulcan® XC-72 (33). A reduced electrolysis cell voltage (1.67 V *vs*. 1.72 V at 1 A cm^{-2} and 90°C) was obtained using Pt/GNF cathodes instead of Pt/XC-72 with the same platinum content (40 wt%).

However, the use of carbon supports for stabilising atomic-scale platinum is challenging because the interaction of the support with platinum atoms must be controlled. Recently, an ultra-low loading of platinum dispersed on single walled carbon nanotubes (SWNTs) (0.19–0.75 at% platinum and a platinum loading of ~114–570 ng_{Pt} cm^{-2}, respectively) was reported in a three-electrode cell with promising properties in terms of electrocatalytic activity and durability for HER in acidic liquid electrolyte (34). More recently, an electrocatalyst comprising platinum nanowires on SWNTs with ultralow platinum content (340 ng_{Pt} cm^{-2}) has been used for HER (35). A comparable activity (10 mA cm^{-2} at −18 mV *vs*. reversible hydrogen electrode (RHE)) to that of state-of-the-art Pt/C (10 mA cm^{-2} at −16 mV *vs*. RHE) was reached in acidic aqueous electrolyte. However, it is worth mentioning that HER kinetics cannot be measured accurately in acidic media, because it is limited entirely by hydrogen diffusion (36) which requires suitable gas transport techniques (37). In fact, PEMWE single cell tests recorded at 55°C using Nafion® 115 membrane and 0.02 mg cm^{-2} of Pt/C or Pt/SWNT at the cathode, while having 3 mg cm^{-2} of $IrRuO_x$ at the anode, revealed similar activity. However, the stability of the electrolyser setup operating the cell at the constant current density of 1 A cm^{-2} was better for the MEA containing the Pt/SWNT catalyst.

The hydrogen and oxygen permeation between cathode and anode through the membranes of the PEMWEs has been investigated (38–40) and although oxygen permeation is lower than that of hydrogen, it increased with current density and temperature, as did hydrogen permeation. The oxygen content in the hydrogen product was found to be three to four times greater when using platinum-free instead of platinum cathode catalysts (39). This was explained by the lower activity for the oxygen reduction using the platinum-free catalyst, so that less permeated oxygen was reduced at the cathode of the PEMWE and consequently, the oxygen flow within hydrogen was higher. It has also been reported that permeated oxygen can be reduced to hydrogen peroxide at the cathode (two-electron reaction), which can be further transformed into hydroxyl radicals, $OH^{\bullet}$, through Fenton's reaction with active metal ion impurities (such as Fe^{2+} and Cu^{2+}) (40). These radicals produce membrane degradation.

2.2 Platinum-Based Catalysts Supported on Non-Carbon Materials

Carbon oxidation of oxygen cathodes has been reported in polymer electrolyte fuel cells (40, 41) and could also be expected in PEMWEs under certain conditions. It is therefore interesting to explore non-carbonaceous supports with high specific surface area. Titania has demonstrated very good chemical resistance and thermal stability (42). Shi *et al*. (43) found that when using a carbon-free Pt/TiO_2 cathode in a PEMWE, the membrane degradation rate was lower compared to a Pt/C cathode. This was explained by the higher rate of hydrogen peroxide generation on the carbon surface of the latter, which led to the formation of $OH^{\bullet}$ and $OOH^{\bullet}$ radicals responsible for membrane degradation by reaction with residual active ions such as Fe^{2+}.

Platinum NPs supported on nitrogen-doped black titania (Pt/N_x:TiO_{2-x}) have been reported to show robust durability and onset potentials for the HER which were somewhat smaller than those of commercial Pt/C catalyst (44). Different platinum catalysts supported on niobium-doped titania nanotubes (TNTs) have been synthesised and tested for the HER in acidic media (45). They showed better electrochemical performance for HER in acidic aqueous solution than those reported in recent literature for synthesised and commercial platinum supported catalysts. These results make Pt/Nb-TNT catalysts, in particular those containing 3 at% niobium, very promising for the HER in PEMWEs.

2.3 Platinum-Based Alloy Catalysts

A further way to reduce the platinum loading in the cathode is by developing active platinum-based alloys. An example is a recently developed platinum-iron alloy stabilised with platinum-skin layers supported on carbon black for HER in acidic media (46). The performance and durability of this catalyst were examined in a PEMWE single cell, which incorporated a MEA consisting of Pt_{xAL}–PtFe/C (0.20 mg_{Pt} cm^{-2}) and a conventional anode IrO_2 + platinum black (0.92 mg_{Pt+Ir} cm^{-2}). The

electrolyte membrane was commercial Nafion® NRE212 (50 μm thick). The initial cell voltage was 1.57 V at 1.0 A cm^{-2} and 80°C and presented an average degradation rate of ~70 μV h^{-1} after 1000 h of continuous operation. This relatively high degradation rate at rather moderate operating conditions was mainly due to the anode, since the cathode operated stably with low H_2O_2 production (the cathode potential varied only ~10 mV during this operating time). The challenge in the case of noble metal-based bimetallic structures is that they may change during the reaction (47).

There is, of course, an alternative way to decrease the cathode platinum loading. Optimising the MEA manufacture would lead to optimal use of the catalyst and, by extension, the cell performance (25). The PEMWE durability at low catalyst loadings is then the issue. Highly active sites may result from synergistic effects between the supporting materials and the electronic properties of the metal when downsizing to single-atom catalysts, as shown in three-electrode cells (47, 48). However, the undesirable tendency to aggregation remains to be solved.

3. Catalysts for the Oxygen Evolution Reaction

Even though the electrochemical splitting of water has been known since the 19th century, more knowledge is needed to understand the OER mechanism and to find the ideal catalyst in terms of activity and stability (49). For large-scale production of water electrolysers, the development of highly active, stable and inexpensive OER catalysts is critical (50).

Due to the sluggish kinetics and the highly oxidative and acidic conditions of the OER, the electrocatalysts used on the anode side must be noble metal-based, mainly iridium and ruthenium, because they show the best performance in terms of activity and stability in the operation conditions (51–53). Considering the industrial importance of PEMWEs, several studies on electrocatalytic properties of iridium- and ruthenium-based catalysts on OER performance in acidic media are discussed in a large body of literature (31, 49, 52–54).

Metallic ruthenium and RuO_2 are known to be the most active catalysts for the OER in acidic media (51, 55, 56). However, several studies have determined that ruthenium has low stability compared to iridium and other metals, even under mild operation conditions (53, 57, 58). Danilovic *et al*. (58) used X-ray absorption spectroscopy together with potentiodynamic OER measurements to establish a functional link between activity and stability of monometallic oxides during the OER in acidic media. They found that the most active oxides (gold ≫ platinum < iridium < ruthenium ≫ osmium) were, in fact, the least stable (gold ≫ platinum > iridium > ruthenium ≫ osmium) materials. Discarding osmium because of its very low stability, RuO_2 also degrades during OER in acidic media. At potentials higher than 1.4 V, the oxidation of RuO_2 to non-conductive RuO_4 is favoured and tends to dissolve rapidly (53, 59). Therefore, this reaction greatly modifies RuO_2 properties, significantly losing its electrocatalytic activity and stability during extended PEMWE operation (52).

A comparative study carried out during OER using an electrochemical scanning flow cell connected to an inductively coupled plasma mass spectrometer, revealed that IrO_2 was more stable than RuO_2, with a difference in dissolution of *ca*. 30 times under similar conditions (53). IrO_2 still has outstanding activity and stability and, for this reason, is used as the state-of-the-art catalyst in PEMWE systems (14, 54).

Unfortunately, the loading of iridium in the anode is significantly higher than the noble metal in the cathode due to the sluggish OER kinetics and stability issue. Moreover, iridium is extremely rare and expensive. For relatively small systems (kilowatt range), the iridium and platinum catalysts comprise about 5–10% of the stack cost (60). The catalyst cost is expected to increase for larger systems (megawatt range), whereas the cost of the other stack components will be lower (61). Therefore, reducing the loading of precious metals, while maintaining higher activity and optimal stability, is critical to enable large-scale implementation of PEMWEs. For the anode, several strategies are currently pursued, such as reducing the particle size and assuring uniform distribution over a conductive support to make all nanoparticles electrochemically accessible. When the particle size is reduced (for a given catalyst loading), the effective surface area is increased and thus, more active sites for the OER are formed (62, 63).

3.1 Iridium-Based Core-Shell Catalysts

In a similar way to platinum, the combination of IrO_2 with other metals in core-shell structures allows

less iridium to be used and, in addition, can display a superior OER activity. Tackett *et al*. (64) described FeN_3 core-IrO_2 shell structures with superior OER activity in which the nitride was protected from the acidic media by the shell. The activity increase was related to electronic effects of the substrate-surface interaction. Nong *et al*. (65) prepared an electrochemically dealloyed IrNi core-IrO_x shell combined with a mesoporous corrosion-resistant antimony-doped tin oxide support (antimony-tin oxide (ATO)), which behaved as highly efficient and stable OER catalysts in acidic medium. The higher OER activity on both geometric surface and iridium-mass basis compared to the IrO_x/C and IrO_x/ATO benchmarks was explained by electronic and strain effects, which could modify the chemisorption and reactivity of intermediates at the surface. More recently, Jiang *et al*. (66) electrodeposited thin iridium films (~68 nm thick) on WO_x nanorods, thus allowing a uniform iridium dispersion on the poorly conducting WO_x and the use of a low loading of the precious metal. Current densities of 2.2 A cm^{-2} were obtained at 2.0 V in a laboratory PEMWE with improved stability over 1000 h at 0.5 A cm^{-2} for a reduced loading of 0.14 mg_{Ir} cm^{-2}, which was assigned to the stability of WO_x and the fixed iridium coating.

3.2 Iridium-Based Catalysts with Metal Oxides

IrO_2 can also be mixed with different metal oxides to create electrocatalysts with improved activity and stability for the OER such as $Ru_xIr_{1-x}O_2$ (59), $Ru_{60}Pt_{30}Ir_{10}$ (67), $Ir_{0.7}Ru_{0.3}O_x$ (68–70) and $Ir_{0.40}Sn_{0.30}Nb_{0.30}O_2$ (71). Computational studies have revealed that the superiority of these mixed metal oxides is due to the stable formation of the intermediates involved in the OER mechanism (72–75). Tang *et al*. (76) found that by switching the host structure of the Ir^{4+} oxygen-coordination octahedra from corner- and edge-sharing rutile (IrO_2) to purely corner-sharing perovskite ($SrIrO_3$), the OER activity increased by more than one order of magnitude. Density functional theory calculations revealed that the adsorption energetics on $SrIrO_3$ depended sensitively on the electron-electron interaction, whereas for IrO_2, it depended rather weakly. Yang *et al*. (77) reported high-activity face-sharing perovskite structures. Despite that the 6H-$SrIrO_3$ perovskite contained 27.1 wt% less iridium than IrO_2, its iridium mass activity was seven times greater than the latter due to the existence of face-sharing IrO_6 octahedral dimers, which facilitated the OER rate determining step by weakening the iridium-oxygen binding.

Another promising solution to decrease the iridium amount is the use of one-dimensional nanoarray electrodes, which shows promise in high catalyst utilisation and enhanced electron and mass transfer (78–80). Zhao *et al*. (80) prepared IrO_x nanotube arrays by electrodepositing IrO_2 NPs onto ZnO nanorod surfaces to produce IrO_2-coated core–shell nanorod arrays, followed by wet chemical etching the ZnO nanorods away. The IrO_x nanotube arrays showed 2.7 times higher turnover frequency (TOF) than that of commercial IrO_2 NPs in the OER. Lu *et al*. (78) prepared vertically aligned IrO_x nanoarrays by electrodeposition using titania nanotube arrays as templates. IrO_x open-end nanotube arrays with tunable length range were obtained by modulating the scan rate in the electrodeposition process. IrO_x nanoarrays performed almost the same OER current density with one twentieth iridium loading amount compared with commercial IrO_2 NPs.

3.3 Iridium-Based Nanostructured Thin Film Catalysts

Another strategy to improve the electrochemically active surface area was the preparation of iridium-based nanostructured thin film (NSTF) electrodes, developed by 3M, USA, which are less sensitive to agglomeration and corrosion due to the special catalyst morphology (21, 81–83). The NSTF catalysts were obtained by physical vapour deposition (PVD) of catalysts onto a supported monolayer of oriented crystalline organic-pigment whiskers. Whiskers are corrosion resistant, therefore eliminating the high voltage corrosion affecting most carbon supports (31). Lewinski *et al*. (81) prepared an ultra-thin continuous film of iridium deposited on arrays of organic nanowhiskers (PR149). NSTF was shown to be able to operate at 0.25 mg_{Ir} cm^{-2} and attain high current densities of 10 A cm^{-2} at ~2 V at 80°C.

More recently, Jensen *et al*. (83) reported the use of a modified PVD technique to prepare interconnected nanoporous thin films by selective leaching of heterogeneous Ir–Co templates formed by an alternating magnetron sputtering process. This approach allowed the preparation of extended surface area catalysts with higher porosity and iridium dispersion, while maintaining high intrinsic activities. Mirshekari *et al*. (84) used reactive spray deposition technology, a flame-based process in which catalyst nanoparticles are synthesised by combusting solutions of metal-organic precursors

in combustible solvents, to fabricate MEAs with very small amounts of catalyst. Anode and cathode contained only 0.3 mg_{Ir} cm^{-2} (in the form of Ir/IrO_x NPs) and 0.2 mg_{Pt} cm^{-2} (platinum NPs on Vulcan XC-72R), respectively. With the purpose of reducing the hydrogen crossover, the MEA contained a thin platinum recombination layer (RL) 100–200 nm in thickness (0.025 mg_{Pt} cm^{-2}) between the Nafion® 211 and the Nafion® 117 membranes of the anode and cathode, respectively. The cell operated for 3000 h at 50°C with 1.8 A cm^{-2} with no significant losses in performance.

3.4 Iridium-Based Catalysts Supported on Conductive Materials

One of the most remarkable ways to achieve highly active electrode with low loading amount of iridium content is the use of conductive supports (67, 85–88). It has been shown that supports are important not only to increase the active surface area of the catalysts, but also to integrate the catalyst-support feature or to improve the charge transfer efficiency between them (89). Stability under the harsh conditions of the cell is one of the main requirements that catalyst supports should meet.

Conductive supports based on carbon materials are routinely used in fuel cell technology. However, under the high potential of the OER, most carbons are easily corroded. Better results were obtained using advanced carbon supports such as carbon nanobowls (90) and nanotubes (91). The stability and activity of iridium nanocrystals supported on carbon nanobowls during the OER at 10 mA cm^{-2} in 0.1 M $HClO_4$ significantly outperformed that of commercial Ir/C (80). IrO_2 supported on carbon nanotubes also exhibited similar stability during the OER at the same current density in 0.1 M H_2SO_4 (88).

3.5 Iridium-Based Catalysts Supported on Metal Oxides

Alternatively, oxide-based supports such as titania (89, 92–94), Ti_4O_7 Magneli phases (70, 95–98) and doped tin oxide (60, 85, 87, 99–101) have been proposed.

3.5.1 Titania-Based Supports

Titania supports offer low cost, very high thermal and chemical stability under anode conditions and commercial availability. However, titania suffers low electric conductivity (about 10^{-6} S cm^{-1} at T < 200°C) and low adsorption/desorption capability toward the species and charge in the OER (31, 102–104). Fuentes *et al*. (92) developed IrRu(1:1) electrocatalysts supported on anatase titania with high activity towards the OER, which showed a 53% higher current per gram of metal than that of unsupported electrocatalyst of the same composition. The higher catalyst utilisation of supported electrocatalysts for the OER was consistent with small, well-dispersed nanoparticles. Mazúr *et al*. (102) prepared IrO_2 NPs (60 wt%) supported on commercial titania powders, with specific surface areas from 10 m^2 g^{-1} to 90 m^2 g^{-1}. They found that the lower the specific surface area of the support the higher was the electrochemical activity of the catalyst. This was explained by the formation of a thin layer of more conductive IrO_2 on the surface of the non-conductive titania, which was able to cover the support with low specific surface area, thus providing the entire material with enough electron conductivity. Rozain *et al*. (105) synthesised IrO_2 catalysts on micro-sized titanium particles (50 wt% titanium), showing that for IrO_2 loadings less than 0.5 mg_{IrO2} cm^{-2}, the performance of the PEMWE was better than that prepared with unsupported IrO_2.

Assuming that titanium was oxidised to TiO_2 during the OER, Bernt *et al*. studied the influence of the ionomer content (24) and of the iridium loading (25) on the performance of a PEMWE using IrO_2/TiO_2 (75 wt% iridium) as the anode electrocatalyst. The best performance was found for 11.6 wt% of the ionomer (24). The performance losses below and over this value were ascribed to a higher proton conduction resistance and to an oxygen higher mass transport resistance, respectively. The iridium loading was varied between 0.20–5.41 mg_{Ir} cm^{-2}. The optimal performance at operational current densities (≥1 A cm^{-2}) was for 1–2 mg_{Ir} cm^{-2}. The CL became very thin and inhomogeneous when its loading was reduced to <0.5 mg_{Ir} cm^{-2}, resulting in a much higher performance loss than expected based simply on the OER kinetics losses (54). This is illustrated in **Figure 2(a)**, where a scanning electron microscopy (SEM) image of the MEA section is shown. On the anode side, there is a porous transport layer (PTL) made of sintered titanium, which facilitates water transport to the CL, composed of IrO_2/TiO_2 and ionomer. Separated by the Nafion® 212 membrane is the cathode, made of 4.8 wt% Pt/C and ionomer, covered by a carbon paper PTL. The thickness of the iridium-based CL depends on the iridium load, as shown in

Figure 2(b), which shows a couple of examples in the insets. **Figures 3(a)** and **3(b)** depict the cross-sectional and top views in the case of a low iridium loading. **Figures 3(c)** and **3(d)** show schemes of the electrical connections in the case of thick and thin anode CLs, whereas in **Figure 3(e)**, the titanium PTLs have been replaced by a carbon PTL with a microporous layer.

Cheng *et al*. (106) synthesised a composite IrO_x-TiO_2-Ti catalyst with mixed valence iridium species. It was shown that titania was beneficial for the formation of Ir(III) and mixed Ir(III/IV) oxyhydroxides, resulting in a high surface concentration of adsorbed hydroxyl and controllable iridium valence, thus explaining its high OER activity.

Additional durability studies were performed with titania-supported IrO_2 (Elyst Ir75 0480 from Umicore, Belgium) with an iridium loading of $2 mg_{Ir} cm^{-2}$ (107). It was observed that the performance of the MEA electrolyser decreased after cycling the anode potential between ~0 V_{RHE} in the open circuit voltage-periods and high potentials when current was applied to the electrolyser. This degradation was due to the formation of the less conductive hydrous $Ir(OH)_x$ phase and the gradual passivation of the titanium porous transport layer (titanium-PTL), which increased the internal ohmic resistance.

The conductivity of titania could be significantly improved by doping with donor species such as metal ions. The group of Hong and Lv extensively studied the effect of doping the titania support for IrO_2 with vanadium (108), niobium (109, 110), tantalum (111) and tungsten (112) on the physical properties and OER activity of the catalysts. They obtained highly active IrO_2 supported on mesoporous niobium (20 at%)-doped titania with specific surface area of 132 $m^2 g^{-1}$ by means of the modified evaporation-induced self-assembly method (109). The authors found that the majority of the OER activity increase was due to the niobium-doping, which enhanced the specific surface area and surface activity of charge and species transfer.

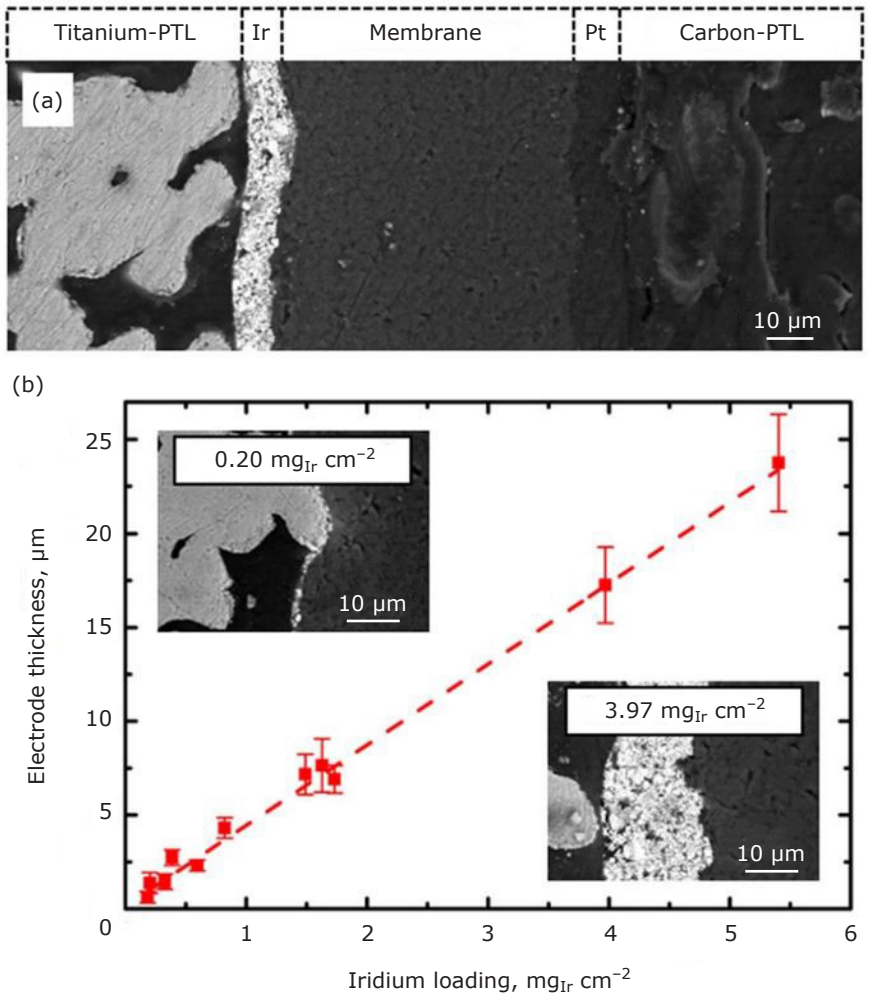

Fig. 2. (a) SEM image of the cross-section of a MEA showing an IrO_2/TiO_2 + ionomer anode CL and a Pt/C + ionomer cathode CL, separated by a Nafion® 212 membrane. The anode and the cathode PTLs were made of titanium and carbon paper, respectively; (b) anode thickness as a function of the iridium loading, with two SEM cross-sectional pictures for different thicknesses as insets. Reproduced from (25) under Creative Commons Attribution 4.0 License (CC BY)

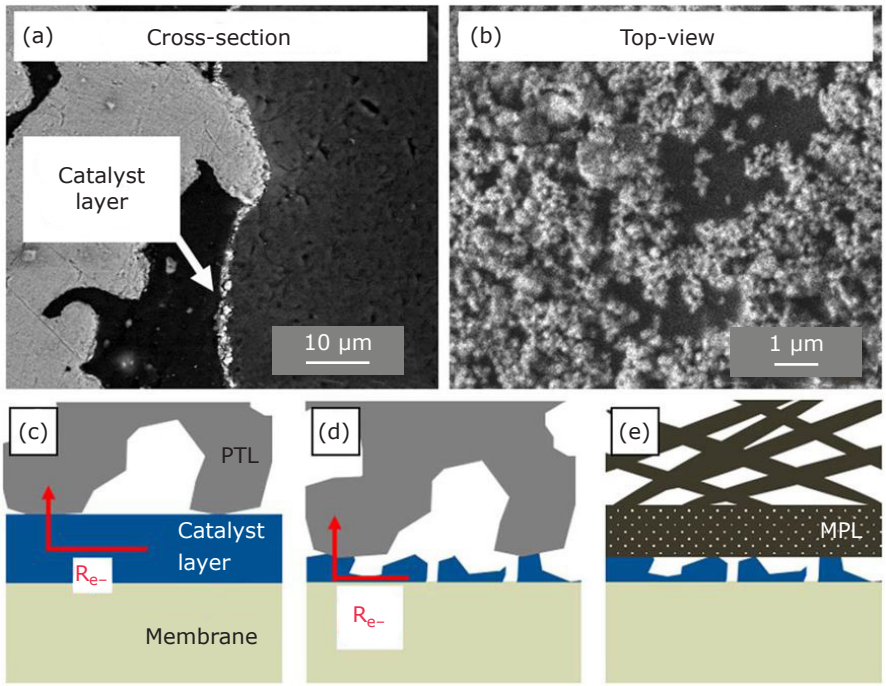

Fig. 3. (a) Cross section; and (b) top-view SEM images of thin iridium-based CLs. The schemes illustrating the electronic transport between the titanium PTLs and the CLs are shown in: (c) for thick; and (d) thin CLs. In (e), the titanium-based PTLs have been replaced by a carbon PTL with a MPL. Reproduced from (25) under Creative Commons Attribution 4.0 License (CC BY)

Subsequent treatment of niobium-doped titania with hydrogen resulted in higher electrical conductivity, increased surface active sites and enhanced OER performance (110). Single cell tests showed that the catalyst treated in hydrogen at 750°C led to the optimum OER activity (1.832 V at 1 A cm^{-2}), which was superior to that of unsupported IrO_2 (1.858 V at 1 A cm^{-2}) and remained stable for 100 h operating at a current density of 1 A cm^{-2}.

They also studied the effect of vanadium doping of the titania support, synthesised by a modified evaporation-induced self-assembly technique (108). IrO_2 supported on titania samples doped with different amounts of vanadium (0 at%, 10 at%, 20 at% and 30 at%) were evaluated. In a single cell, the OER performance gradually increased with vanadium dopant from 0 at% to 20 at%, followed by a performance deterioration with vanadium amount reaching 30 at% due to the corrodible V_2O_5 precipitate. Recently, the incorporation of tungsten to obtain $IrO_2/Ti_{1-x}W_xO_2$ (x = 0.05, 0.1 and 0.2), resulted in an active electrocatalyst for the OER. Of all the $Ti_{1-x}W_xO_2$ supports, the highest electrocatalytic activity was obtained with $Ti_{0.9}W_{0.1}O_2$. With optimised IrO_2 loading, the applied potential in a single water electrolysis cell was 1.79 V to obtain 1 A cm^{-2} at 80°C. Durability tests for $40IrO_2/Ti_{0.9}W_{0.1}O_2$ at 0.5 A cm^{-2} and 1 A cm^{-2} indicated that the cell voltages were stable over 100 h.

Hu *et al*. (113) synthetised IrO_2 dispersed on a corrosion-resistant $Nb_{0.05}Ti_{0.95}O_2$ support (83 $m^2\ g^{-1}$) by the sol-gel method. The IrO_2 loading of 26 wt% exhibited the best mass normalised OER activity, which was explained by uniform support of the IrO_2 NPs on the surface, thus providing conductive channels to reduce the grain boundary resistance. Recently, Alcaide *et al*. (89) prepared IrO_2 and $IrRuO_x$ (50 wt%) supported on titania nanotubes and niobium-doped titania nanotubes (3 at% niobium). They observed that niobium doping of titania significantly increased the surface area of the support from 145 $m^2\ g^{-1}$ to 260 $m^2\ g^{-1}$. The highest OER performance of IrO_2/Nb-TiO_2 nanotubes was assigned to the good dispersion and accessibility of the IrO_2 NPs, the high specific surface area of the support and the electron donor properties of the Nb^{4+} species to the conduction band of titania. The stability with the Nb-TiO_2 nanotubes was also better than that of unsupported IrO_2.

3.5.2 Ti_nO_{2n-1}-Based Supports

Non-stoichiometric titanium sub-oxides, TiO_{2-x}, have drawn considerable attention due to their high electronic conductivity. In particular, the titanium sub-oxides Magneli phases, Ti_nO_{2n-1}, such as Ti_5O_9 and Ti_4O_7 or a mixture, which are known by the commercial name Ebonex®, are highly conductive and corrosion resistant in acidic media during the OER (95, 96). Metallic iridium NPs supported on Ti_4O_7 were synthetised by Wang *et al*. (86) *via* a conventional sodium borohydride reduction method in anhydrous ethanol at room temperature.

The catalyst exhibited improved OER kinetics in acidic media and higher TOF compared to iridium-black. A study comparing IrO_2 electrocatalysts supported on commercial Ebonex® and titanium-suboxides (Ti_nO_{2n-1}) prepared in-house was carried out by Siracusano *et al*. (114). The results showed expected electronic conductivity for both electrocatalysts and superior OER activity of the catalyst based on titanium-suboxides prepared in-house compared to the commercial support. These results were attributed to better dispersion and larger occurrence of active catalytic sites on the surface of the suboxide prepared in-house.

3.5.3 Antimony-Tin Oxide-Based Supports

ATO has been considered as an alternative support material for OER catalysts because it exhibits relatively high electrical conductivity and corrosion resistance. Some dissolution of the dopant has been reported during the OER at high anodic potentials in sulfuric acid. However, it withstands anodic conditions better than indium-doped tin oxide, known as indium-tin oxide (ITO) (101). Liu *et al*. (115) synthetised antimony-tin oxide nanowires (nw) as supporting materials for IrO_2 NPs which exhibited significant improvement in mass activity when compared to the same catalyst supported on antimony-tin oxide NPs and pure IrO_2. The OER performance was further confirmed by PEMWE tests at 80°C; the IrO_2/ATO-nw catalyst reached 2 A cm^{-2} at 1.62 V *vs*. RHE (80°C) with an activity loss of 0.76 mV h^{-1} after 646 h at 0.45 A cm^{-2}.

Wang *et al*. (116) found that IrO_2 supported on ATO aerogels allowed the use of noble metal to be reduced while keeping the same OER current per unit geometric surface area. Furthermore, the highly porous structure of SnO_2:Sb aerogel was successfully retained by using vanadium additives under atmospheric drying. However, vanadium did not play an active role in OER catalysis. Similarly, iridium NPs supported on SnO_2:Sb aerogel allowed the use of precious metal to be decreased by more than 70% while enhancing the electrocatalytic activity and stability (60). *Operando* near-ambient pressure X-ray photoelectron spectroscopy on MEAs revealed a low degree of iridium oxidation, attributed to the oxygen spill-over from iridium to SnO_2:Sb where the formation of highly unstable Ir^{3+} species was mitigated.

A comprehensive overview of the stability and degradation of catalysts during the OER in acidic media was given by Spöri *et al*. (117). They established that the degree of metal immobilisation on the support depends on the interface between the support surface (groups) and the metal oxide and influences the extent of particle detachment or dissolution during the OER process. These interactions can range from weak electrostatic attraction to stronger connections through surface chemical bonds or formation of an overlayer on the support, which can also affect the activity by decreasing or increasing electron density to the catalyst surface. More recently, several reviews address electrocatalyst performance in terms of activity, stability and efficiency (17, 118, 119). Kim *et al*. (17) have reviewed the latest advances in iridium-based, ruthenium-based and even non-noble metal-based multimetallic electrocatalysts for the OER in acidic media, with emphasis on their stability and reference to machine learning models. Wang *et al*. (118) have summarised the OER performance of selected catalysts in acidic and alkaline media. Also related to this point, an in-depth literature review of the OER mechanism, with special emphasis on the adsorption and lattice oxygen evolution mechanisms to elucidate the catalyst degradation, has recently been published by Chen *et al*. (119).

4. Performance of Selected Proton Exchange Membrane Water Electrolysers

Table I shows the performance of selected PEMWE single cells in recent years, generally at 80°C, including catalyst loading, operating conditions, type of membrane and degradation rate, which have been discussed in this paper. In this review, we have seen many different anodic and cathodic catalysts which have been studied in three-electrode cells and in laboratory PEMWEs. Note that the latter have been generally tested using platinum supported on carbon cathodes and different PEMs, also applying different voltages, resulting in different current densities. It is therefore not easy to extract the best PEMWEs, since changing the anode, the cathode, the membrane, the temperature, the cell voltage or catalyst loadings can lead to significant changes in the cell performance. Optimisation of all these parameters should be performed. However, promising results can be ascertained.

General trends can be observed: (a) current densities and cell voltages are similar, but the most recent papers use less iridium at the anode due to better dispersion of the precious metal, either

https://doi.org/10.1595/205651323X16648726195503

Table I Performance Data of Selected PEMWE Single Cells Made with Different Components Under the Indicated Conditions from 2009 to 2021

Anode		Cathode		Operating conditions					
Catalyst	Loading, mg cm^{-2}	Catalyst	Loading, mg cm^{-2}	Voltage, V	Current density, A cm^{-2}	Temperature, °C	Membrane	Degradation rate	Ref.
Ir/IrO_x	0.3	Pt/C	0.2	2.09	1.8	50	Nafion® 211/Pt RL/ Nafion® 117	24 μV h^{-1}, 1.8 A cm^{-2}, 3000 h	(84)
$Ir@WO_x$	0.14	70 wt% Pt/C	0.4	2.0	2.2	80	Nafion® 115	49.7 μV h^{-1}, 0.5 A cm^{-2}, 1030 h	(66)
IrO_2	1.40	60 wt% Pt/C	0.50	1.80	2.0	80	Nafion® D520	N/A	(15)
IrO_2	0.90	55.5–58.5 wt% Pt/C	0.25	1.80	3.6	80	Nafion® 212	N/A	(26)
RuO_2	3.0	30 wt% Pd/B_3-CNPs	0.70	1.86	0.50	80	Nafion® 115	2.04 V, 500 h, 1 A cm^{-2}	(29)
$Ir_{0.7}Ru_{0.3}O_x$	0.40	40 wt% Pt/C	0.10	1.82	3.0	80	Aquivion® membrane (E98-09S)	90 μV h^{-1}, 800 h	(69)
Ir/SnO_2:Sb	0.50 (Ir)	40 wt% Pt/C	1.0	N/A	N/A	N/A	Aquivion® membrane (E87-05S)	N/A	(60)
IrO_2	1.40	60 wt% Pt/C	0.50	1.80	1.1	80	Nafion® 117	200 h, 2 A cm^{-2}	(22)
$IrO_2/Sb\text{-}SnO_2$ (7/3)	0.50	40 wt% Pt/C	5.00	1.70	~1.3	80	Nafion® 211	N/A	(100)
IrO_2 + Pt black (1:1)	0.92	Pt_{xAL}–PtFe/C	0.20	1.57	1.0	80	Nafion® 212	~70 μV h^{-1}, 1 A cm^{-2}, 1000 h	(46)
IrO_2	2.10	55.5–58.5 wt% Pt/C	0.40	1.80	6.0	80	N/A	N/A	(23)
IrO_2 (75%) / TiO_2	1.50–2.0 (Ir)	4.8 wt% Pt/C	0.025 (Pt)	1.79	3.6	80	Nafion® 212	N/A	(25)
IrO_2 (20%) / gCNH	N/A	Pt/C	4.0 (Pt)	1.80	~0.7	80	Nafion® 115	N/A	(88)
$IrRuO_x$	3.0	Pt black	0.086	1.80	~1.8	80	Nafion® 115	N/A	(30)
Ir black	2.0	Pt/C	1.0	1.80	~1.3	80	Nafion® N115/Pt (0.02 mg cm^{-2})/ Nafion® NR212	190 μV h^{-1}, 1 A cm^{-2}	(19)
IrO_2	2.50	40 wt% Pt/C	0.40	1.70	1.0	90	Nafion® 117	35.5 μV h^{-1}	(32)
40 wt% $IrO_2/V\text{-}TiO_2$ (20 at% V)	2.50	40 wt% Pt/C	0.50	1.80	0.6	80	Nafion® 117	N/A	(108)

(*Continued*)

Table I (*Continued*)

Anode		Cathode		Operating conditions			Membrane	Degradation rate	Ref.
Catalyst	Loading, mg cm^{-2}	Catalyst	Loading, mg cm^{-2}	Voltage, V	Current density, A cm^{-2}	Temperature, °C			
$Ir_{0.7}Ru_{0.3}O_x$	1.0	40 wt% Pt/C	0.40	1.70	1.0	80	Nafion® NR212	81 μV h^{-1}	(70)
IrO_2/Ti (50 wt% Ti)	0.1	46 wt% Pt/C	0.25	1.73	1.0	80	Nafion® NRE 115CS	1000 h, 20 μV h^{-1}	(105)
Ru@Pt (core-shell)	0.10	Pt@WO_3 (core-shell)	0.10	1.80	1.0	80	Nafion® 117	N/A	(61)
IrO_2/Sb-SnO_2 nanowire	0.75	40 wt% Pt/C	0.20	1.62	2.0	80	Nafion® NR212	0.76 mV h^{-1}, 0.45 A cm^{-2} at 35°C	(115)
67 wt% IrO2/Ti_nO_{2n-1}	1.0	30 wt% Pt/Vulcan XC-72	1.0	1.80	0.700	80	Nafion® 115	N/A	(114)

on a supporting material or unsupported, although obtained using a different synthesis procedure; (b) a gain in the PEMWE stability is also seen, with several factors affecting PEMWE stability including anode structure and membrane degradation; and (c) limiting the permeation of gases through the membrane leads to better PEMWE stability since radicals formed at the cathode produce membrane degradation.

5. Concluding Remarks

In this review, an overview of the most recent advances in electrocatalysis for PEM water electrolysis has been provided, both for the HER at the cathode and the OER at the anode, paying special attention to the development of noble metal supported catalysts and their implementation into practical systems. For the former reaction, Pt/C is the most common catalyst, while for the latter the most used catalysts are iridium black and IrO_2. Both noble metals are scarce and expensive. Several approaches to develop highly structured catalysts leading to high metal dispersion and, ultimately, lower loadings at the electrodes have been thoroughly reviewed. Regarding the HER, platinum supported on advanced carbon materials achieves the expected targets in terms of performance, but in the authors' opinion, durability is an issue that requires the use of alternative titanium-based non-carbon supports. Regarding the OER, among the reviewed approaches and also in the authors' opinion, the development of iridium-based catalysts supported on conductive metal oxides such as those based on niobium-doped titania and antimony-doped tin oxide could lead to the expected performance and durability required by industry players.

Overall, in the short term, the development of advanced supports for metal dispersion will allow the use of these noble metals to be optimised, reducing the cost and increasing the performance and durability of the electrolysers. In the long term, the development of non-noble catalysts and their implementation in real cells is mandatory to ensure the viability of the technology. In this sense, preliminary studies carried out with non-noble catalysts in half-cell configuration are promising, but further work is necessary to improve their stability and durability in practical cells. Thus, there is still a long way to go before their implementation in commercial PEMWEs.

References

1. K. Bareiß, C. de la Rua, M. Möckl and T. Hamacher, *Appl. Energy*, 2019, **237**, 862
2. P. C. K. Vesborg and T. F. Jaramillo, *RSC Adv.*, 2012, **2**, (21), 7933
3. M. Pudukudy, Z. Yaakob, M. Mohammad, B. Narayanan and K. Sopian, *Renew. Sustain. Energy Rev.*, 2014, **30**, 743
4. P. Nikolaidis and A. Poullikkas, *Renew. Sustain. Energy Rev.*, 2017, **67**, 597
5. Y. Naimi and A. Antar, 'Hydrogen Generation by Water Electrolysis', in "Advances in Hydrogen Generation Technologies", ed. M. Eyvaz, Ch. 1, InTechOpen, London, UK, 2018, 18 pp
6. D. M. F. Santos, C. A. C. Sequeira and J. L. Figueiredo, *Quim. Nova*, 2013, **36**, (8), 1176
7. D. Berndt and D. Spahrbier, 'Batteries', in "Ullmann's Encyclopedia of Industrial Chemistry", Wiley-VCH Verlag GmbH, Weinheim, Germany, 2005
8. J. Brauns and T. Turek, *Processes*, 2020, **8**, (2), 248
9. A. S. Aricò, S. Siracusano, N. Briguglio, V. Baglio, A. Di Blasi and V. Antonucci, *J. Appl. Electrochem.*, 2013, **43**, (2), 107
10. X. Sun, K. Xu, C. Fleischer, X. Liu, M. Grandcolas, R. Strandbakke, T. S. Bjørheim, T. Norby and A. Chatzitakis, *Catalysts*, 2018, **8**, (12), 657
11. A. Kusoglu and A. Z. Weber, *Chem. Rev.*, 2017, **117**, (3), 987
12. P. Millet, N. Mbemba, S. A. Grigoriev, V. N. Fateev, A. Aukauloo and C. Etiévant, *Int. J. Hydrogen Energy*, 2011, **36**, (6), 4134
13. M. Suermann, B. Bensmann and R. Hanke-Rauschenbach, *J. Electrochem. Soc.*, 2019, **166**, (10), F645
14. P. Shirvanian and F. van Berkel, *Electrochem. Commun.*, 2020, **114**, 106704
15. P. Holzapfel, M. Bühler, C. Van Pham, F. Hegge, T. Böhm, D. McLaughlin, M. Breitwieser and S. Thiele, *Electrochem. Commun.*, 2020, **110**, 106640
16. T. Reier, M. Oezaslan and P. Strasser, *ACS Catal.*, 2012, **2**, (8), 1765
17. T. Kim, B. Kim, T. Kwon, H. Y. Kim, J. Y. Kim and K. Lee, *Mater. Chem. Front.*, 2021, **5**, (12), 4445
18. K. Ayers, N. Danilovic, R. Ouimet, M. Carmo, B. Pivovar and M. Bornstein, *Annu. Rev. Chem. Biomol. Eng.*, 2019, **10**, 219
19. C. Klose, P. Trinke, T. Böhm, B. Bensmann, S. Vierrath, R. Hanke-Rauschenbach and S. Thiele, *J. Electrochem. Soc.*, 2018, **165**, (16), F1271
20. J. Hu, J. Luo, P. Wagner, O. Conrad and C. Agert, *Electrochem. Commun.*, 2009, **11**, (12), 2324
21. Q. Feng, X.-Z. Yuan, G. Liu, B. Wei, Z. Zhang, H. Li and H. Wang, *J. Power Sources*, 2017, **366**, 33
22. M. Bühler, F. Hegge, P. Holzapfel, M. Bierling, M. Suermann, S. Vierrath and S. Thiele, *J. Mater. Chem. A*, 2019, **7**, (47), 26984
23. M. Stähler, A. Stähler, F. Scheepers, M. Carmo and D. Stolten, *Int. J. Hydrogen Energy*, 2019, **44**, (14), 7053
24. M. Bernt and H. A. Gasteiger, *J. Electrochem. Soc.*, 2016, **163**, (11), F3179
25. M. Bernt, A. Siebel and H. A. Gasteiger, *J. Electrochem. Soc.*, 2018, **165**, (5), F305
26. M. Stähler, A. Stähler, F. Scheepers, M. Carmo, W. Lehnert and D. Stolten, *Int. J. Hydrogen Energy*, 2020, **45**, (7), 4008
27. M. Bajdich, M. García-Mota, A. Vojvodic, J. K. Nørskov and A. T. Bell, *J. Am. Chem. Soc.*, 2013, **135**, (36), 13521
28. S. S. Kumar and V. Himabindu, *Mater. Sci. Energy Technol.*, 2019, **2**, (3), 442
29. S. S. Kumar and V. Himabindu, *Renew. Energy*, 2020, **146**, 2281
30. Z. Kang, G. Yang, J. Mo, Y. Li, S. Yu, D. A. Cullen, S. T. Retterer, T. J. Toops, G. Bender, B. S. Pivovar, J. B. Green and F.-Y. Zhang, *Nano Energy*, 2018, **47**, 434
31. M. Carmo, D. L. Fritz, J. Mergel and D. Stolten, *Int. J. Hydrogen Energy*, 2013, **38**, (12), 4901
32. S. A. Grigoriev and A. A. Kalinnikov, *Int. J. Hydrogen Energy*, 2017, **42**, (3), 1590
33. S. A. Grigoriev, M. S. Mamat, K. A. Dzhus, G. S. Walker and P. Millet, *Int. J. Hydrogen Energy*, 2011, **36**, (6), 4143
34. M. Tavakkoli, N. Holmberg, R. Kronberg, H. Jiang, J. Sainio, E. I. Kauppinen, T. Kallio and K. Laasonen, *ACS Catal.*, 2017, **7**, (5), 3121
35. T. Rajala, R. Kronberg, R. Backhouse, M. E. M. Buan, M. Tripathi, A. Zitolo, H. Jiang, K. Laasonen, T. Susi, F. Jaouen and T. Kallio, *Appl. Catal. B: Environ.*, 2020, **265**, 118582
36. W. Sheng, H. A. Gasteiger and Y. Shao-Horn, *J. Electrochem. Soc.*, 2010, **157**, (11), B1529
37. C. M. Zalitis, D. Kramer and A. R. Kucernak, *Phys. Chem. Chem. Phys.*, 2013, **15**, (12), 4329
38. E. Price, *Johnson Matthey Technol. Rev.*, 2017, **61**, (1), 47
39. P. Trinke, B. Bensmann and R. Hanke-Rauschenbach, *Electrochem. Commun.*, 2017, **82**, 98

40. M. Chandesris, V. Médeau, N. Guillet, S. Chelghoum, D. Thoby and F. Fouda-Onana, *Int. J. Hydrogen Energy*, 2015, **40**, (3), 1353
41. A. A. Franco and M. Gerard, *J. Electrochem. Soc.*, 2008, **155**, (4), B367
42. X. Chen and S. S. Mao, *Chem. Rev.*, 2007, **107**, (7), 2891
43. Y. Shi, L. Guo, Z. Lu, Z. Wang, Y. Gan, C. Guo, H. Tan and C. Yan, *Energy Technol.*, 2019, **7**, (5), 1800781
44. X. Wang, X. Yuan, X. Liu, W. Dong, C. Dong, M. Lou, J. Li, T. Lin and F. Huang, *J. Alloys Compd.*, 2017, **701**, 669
45. F. Alcaide, R. V. Genova, G. Álvarez, H.-J. Grande, Ó. Miguel and P. L. Cabot, *Int. J. Hydrogen Energy*, 2020, **45**, (40), 20605
46. G. Shi, H. Yano, D. A. Tryk, S. Nohara and H. Uchida, *Phys. Chem. Chem. Phys.*, 2019, **21**, (6), 2861
47. C. Li and J.-B. Baek, *ACS Omega*, 2020, **5**, (1), 31
48. N. Cheng, S. Stambula, D. Wang, M. N. Banis, J. Liu, A. Riese, B. Xiao, R. Li, T.-K. Sham, L.-M. Liu, G. A. Botton and X. Sun, *Nat. Commun.*, 2016, **7**, 13638
49. E. Fabbri and T. J. Schmidt, *ACS Catal.*, 2018, **8**, (10), 9765
50. N.-T. Suen, S.-F. Hung, Q. Quan, N. Zhang, Y.-J. Xu and H. M. Chen, *Chem. Soc. Rev.*, 2017, **46**, (2), 337
51. S. Trasatti, *Electrochim. Acta*, 1984, **29**, (11), 1503
52. S. Park, Y. Shao, J. Liu and Y. Wang, *Energy Environ. Sci.*, 2012, **5**, (11), 9331
53. S. Cherevko, S. Geiger, O. Kasian, N. Kulyk, J.-P. Grote, A. Savan, B. R. Shrestha, S. Merzlikin, B. Breitbach, A. Ludwig and K. J. J. Mayrhofer, *Catal. Today*, 2016, **262**, 170
54. M. Bernt, A. Hartig-Weiß, M. F. Tovini, H. A. El-Sayed, C. Schramm, J. Schröter, C. Gebauer and H. A. Gasteiger, *Chem. Ing. Tech.*, 2020, **92**, (1–2), 31
55. C. Iwakura, K. Hirao and H. Tamura, *Electrochim. Acta*, 1977, **22**, (4), 329
56. E. A. Paoli, F. Masini, R. Frydendal, D. Deiana, C. Schlaup, M. Malizia, T. W. Hansen, S. Horch, I. E. L. Stephens and I. Chorkendorff, *Chem. Sci.*, 2015, **6**, (1), 190
57. M. Escudero-Escribano, A. F. Pedersen, E. A. Paoli, R. Frydendal, D. Friebel, P. Malacrida, J. Rossmeisl, I. E. L. Stephens and I. Chorkendorff, *J. Phys. Chem. B*, 2018, **122**, (2), 947
58. N. Danilovic, R. Subbaraman, K.-C. Chang, S. H. Chang, Y. J. Kang, J. Snyder, A. P. Paulikas, D. Strmcnik, Y.-T. Kim, D. Myers, V. R. Stamenkovic and N. M. Markovic, *J. Phys. Chem. Lett.*, 2014, **5**, (14), 2427
59. R. Kötz and S. Stucki, *Electrochim. Acta*, 1986, **31**, (10), 1311
60. V. A. Saveleva, L. Wang, O. Kasian, M. Batuk, J. Hadermann, J.-J. Gallet, F. Bournel, N. Alonso-Vante, G. Ozouf, C. Beauger, K. J. J. Mayrhofer, S. Cherevko, A. S. Gago, K. A. Friedrich, S. Zafeiratos and E. R. Savinova, *ACS Catal.*, 2020, **10**, (4), 2508
61. K. E. Ayers, J. N. Renner, N. Danilovic, J. X. Wang, Y. Zhang, R. Maric and H. Yu, *Catal. Today*, 2016, **262**, 121
62. X. Xia, L. Figueroa-Cosme, J. Tao, H.-C. Peng, G. Niu, Y. Zhu and Y. Xia, *J. Am. Chem. Soc.*, 2014, **136**, (31), 10878
63. S. Siracusano, V. Baglio, S. A. Grigoriev, L. Merlo, V. N. Fateev and A. S. Aricò, *J. Power Sources*, 2017, **366**, 105
64. B. M. Tackett, W. Sheng, S. Kattel, S. Yao, B. Yan, K. A. Kuttiyiel, Q. Wu and J. G. Chen, *ACS Catal.*, 2018, **8**, (3), 2615
65. H. N. Nong, H.-S. Oh, T. Reier, E. Willinger, M.-G. Willinger, V. Petkov, D. Teschner and P. Strasser, *Angew. Chem. Int. Ed.*, 2015, **54**, (10), 2975
66. G. Jiang, H. Yu, Y. Li, D. Yao, J. Chi, S. Sun and Z. Shao, *ACS Appl. Mater. Interfaces,* 2021, **13**, (13), 15073
67. K. C. Neyerlin, G. Bugosh, R. Forgie, Z. Liu and P. Strasser, *J. Electrochem. Soc.*, 2009, **156**, (3), B363
68. S. Siracusano, N. Van Dijk, E. Payne-Johnson, V. Baglio and A. S. Aricò, *Appl. Catal. B: Environ.*, 2015, **164**, 488
69. S. Siracusano, S. Trocino, N. Briguglio, F. Pantò and A. S. Aricò, *J. Power Sources*, 2020, **468**, 228390
70. L. Wang, V. A. Saveleva, S. Zafeiratos, E. R. Savinova, P. Lettenmeier, P. Gazdzicki, A. S. Gago and K. A. Friedrich, *Nano Energy*, 2017, **34**, 385
71. K. Kadakia, M. K. Datta, O. I. Velikokhatnyi, P. Jampani, S. K. Park, P. Saha, J. A. Poston, A. Manivannan and P. N. Kumta, *Int. J. Hydrogen Energy*, 2012, **37**, (4), 3001
72. I. C. Man, H.-Y. Su, F. Calle-Vallejo, H. A. Hansen, J. I. Martínez, N. G. Inoglu, J. Kitchin, T. F. Jaramillo, J. K. Nørskov and J. Rossmeisl, *ChemCatChem*, 2011, **3**, (7), 1159
73. A. Eftekhari, *Mater. Today Energy*, 2017, **5**, 37
74. J. Rossmeisl, Z.-W. Qu, H. Zhu, G.-J. Kroes and J. K. Nørskov, *J. Electroanal. Chem.*, 2007, **607**, (1–2), 83
75. M. T. M. Koper, *J. Electroanal. Chem.*, 2011,

660, (2), 254

76. R. Tang, Y. Nie, J. K. Kawasaki, D.-Y. Kuo, G. Petretto, G. Hautier, G.-M. Rignanese, K. M. Shen, D. G. Schlom and J. Suntivich, *J. Mater. Chem. A*, 2016, **4**, (18), 6831
77. L. Yang, G. Yu, X. Ai, W. Yan, H. Duan, W. Chen, X. Li, T. Wang, C. Zhang, X. Huang, J.-S. Chen and X. Zou, *Nat. Commun.*, 2018, **9**, 5236
78. Z.-X. Lu, Y. Shi, P. Gupta, X. Min, H. Tan, Z.-D. Wang, C. Guo, Z. Zou, H. Yang, S. Mukerjee and C.-F. Yan, *Electrochim. Acta*, 2020, **348**, 136302
79. Q. Shi, C. Zhu, D. Du, J. Wang, H. Xia, M. H. Engelhard, S. Feng and Y. Lin, *J. Mater. Chem. A*, 2018, **6**, (19), 8855
80. C. Zhao, H. Yu, Y. Li, X. Li, L. Ding and L. Fan, *J. Electroanal. Chem.*, 2013, **688**, 269
81. K. A. Lewinski, D. van der Vliet and S. M. Luopa, *ECS Trans.*, 2015, **69**, (17), 893
82. R. T. Atanasoski, L. L. Atanasoska, D. A. Cullen, G. M. Haugen, K. L. More and G. D. Vernstrom, *Electrocatalysis*, 2012, **3**, (3–4), 284
83. A. W. Jensen, G. W. Sievers, K. D. Jensen, J. Quinson, J. A. Arminio-Ravelo, V. Brüser, M. Arenz and M. Escudero-Escribano, *J. Mater. Chem. A*, 2020, **8**, (3), 1066
84. G. Mirshekari, R. Ouimet, Z. Zeng, H. Yu, S. Bliznakov, L. Bonville, A. Niedzwiecki, C. Capuano, K. Ayers and R. Maric, *Int. J. Hydrogen Energy*, 2021, **46**, (2), 1526
85. H.-S. Oh, H. N. Nong, T. Reier, M. Gliech and P. Strasser, *Chem. Sci.*, 2015, **6**, (6), 3321
86. L. Wang, P. Lettenmeier, U. Golla-Schindler, P. Gazdzicki, N. A. Cañas, T. Morawietz, R. Hiesgen, S. S. Hosseiny, A. S. Gago and K. A. Friedrich, *Phys. Chem. Chem. Phys.*, 2016, **18**, (6), 4487
87. L. Solà-Hernández, F. Claudel, F. Maillard and C. Beauger, *Int. J. Hydrogen Energy*, 2019, **44**, (45), 24331
88. A. B. Jorge, I. Dedigama, T. S. Miller, P. Shearing, D. J. L. Brett and P. F. McMillan, *Nanomaterials*, 2018, **8**, (6), 432
89. R. V. Genova-Koleva, F. Alcaide, G. Álvarez, P. L. Cabot, H.-J. Grande, M. V. Martínez-Huerta and O. Miguel, *J. Energy Chem.*, 2019, **34**, 227
90. Q. Xue, W. Gao, J. Zhu, R. Peng, Q. Xu, P. Chen and Y. Chen, *J. Colloid Interface Sci.*, 2018, **529**, 325
91. R. Badam, M. Hara, H.-H. Huang and M. Yoshimura, *Int. J. Hydrogen Energy*, 2018, **43**, (39), 18095
92. R. E. Fuentes, J. Farell and J. W. Weidner, *Electrochem. Solid-State Lett.*, 2011, **14**, (3), E5
93. M. García-Mota, A. Vojvodic, H. Metiu, I. C. Man, H.-Y. Su, J. Rossmeisl and J. K. Nørskov, *ChemCatChem*, 2011, **3**, (10), 1607
94. M. Aizawa, S. Lee and S. L. Anderson, *Surf. Sci.*, 2003, **542**, (3), 253
95. F. C. Walsh and R. G. A. Wills, *Electrochim. Acta*, 2010, **55**, (22), 6342
96. S.-S. Huang, Y.-H. Lin, W. Chuang, P.-S. Shao, C.-H. Chuang, J.-F. Lee, M.-L. Lu, Y.-T. Weng and N.-L. Wu, *ACS Sustain. Chem. Eng.*, 2018, **6**, (3), 3162
97. K. Huang, Y. Li and Y. Xing, *J. Mater. Res.*, 2013, **28**, (3), 454
98. A. Kitada, G. Hasegawa, Y. Kobayashi, K. Kanamori, K. Nakanishi and H. Kageyama, *J. Am. Chem. Soc.*, 2012, **134**, (26), 10894
99. M. P. Gurrola, J. Gutiérrez, S. Rivas, M. Guerra-Balcázar, J. Ledesma-García and L. G. Arriaga, *Int. J. Hydrogen Energy*, 2014, **39**, (29), 16763
100. S.-B. Han, Y.-H. Mo, Y.-S. Lee, S.-G. Lee, D.-H. Park and K.-W. Park, *Int. J. Hydrogen Energy*, 2020, **45**, (3), 1409
101. S. Geiger, O. Kasian, A. M. Mingers, K. J. J. Mayrhofer and S. Cherevko, *Sci. Rep.*, 2017, **7**, 4595
102. P. Mazúr, J. Polonský, M. Paidar and K. Bouzek, *Int. J. Hydrogen Energy*, 2012, **37**, (17), 12081
103. Y.-C. Nah, I. Paramasivam and P. Schmuki, *ChemPhysChem*, 2010, **11**, (13), 2698
104. G. Garcia-Belmonte, V. Kytin, T. Dittrlch and J. Bisquert, *J. Appl. Phys.*, 2003, **94**, (8), 5261
105. C. Rozain, E. Mayousse, N. Guillet and P. Millet, *Appl. Catal. B: Environ.*, 2016, **182**, 123
106. J. Cheng, J. Yang, S. Kitano, G. Juhasz, M. Higashi, M. Sadakiyo, K. Kato, S. Yoshioka, T. Sugiyama, M. Yamauchi and N. Nakashima, *ACS Catal.*, 2019, **9**, (8), 6974
107. A. Weiß, A. Siebel, M. Bernt, T.-H. Shen, V. Tileli and H. A. Gasteiger, *J. Electrochem. Soc.*, 2019, **166**, (8), F487
108. C. Hao, H. Lv, Q. Zhao, B. Li, C. Zhang, C. Mi, Y. Song and J. Ma, *Int. J. Hydrogen Energy*, 2017, **42**, (15), 9384
109. C. Hao, H. Lv, C. Mi, Y. Song and J. Ma, *ACS Sustain. Chem. Eng.*, 2016, **4**, (3), 746
110. H. Lv, S. Wang, C. Hao, W. Zhou, J. Li, M. Xue and C. Zhang, *ChemCatChem*, 2019, **11**, (10), 2511

111. H. Lv, G. Zhang, C. Hao, C. Mi, W. Zhou, D. Yang, B. Li and C. Zhang, *RSC Adv.*, 2017, **7**, (64), 40427
112. H. Lv, J. Zuo, W. Zhou, X. Shen, B. Li, D. Yang, Y. Liu, L. Jin and C. Zhang, *J. Electroanal. Chem.*, 2019, **833**, 471
113. W. Hu, S. Chen and Q. Xia, *Int. J. Hydrogen Energy*, 2014, **39**, (13), 6967
114. S. Siracusano, V. Baglio, C. D'Urso, V. Antonucci and A. S. Aricò, *Electrochim. Acta*, 2009, **54**, (26), 6292
115. G. Liu, J. Xu, Y. Wang and X. Wang, *J. Mater. Chem. A*, 2015, **3**, (41), 20791
116. L. Wang, F. Song, G. Ozouf, D. Geiger, T. Morawietz, M. Handl, P. Gazdzicki, C. Beauger, U. Kaiser, R. Hiesgen, A. S. Gago and K. A. Friedrich, *J. Mater. Chem. A*, 2017, **5**, (7), 3172
117. C. Spöri, J. T. H. Kwan, A. Bonakdarpour, D. P. Wilkinson and P. Strasser, *Angew. Chem. Int. Ed.*, 2017, **56**, (22), 5994
118. S. Wang, A. Lu and C.-J. Zhong, *Nano Converg.*, 2021, **8**, 4
119. Z. Chen, L. Guo, L. Pan, T. Yan, Z. He, Y. Li, C. Shi, Z.-F. Huang, X. Zhang and J.-J. Zou, *Adv. Energy Mater.*, 2022, **12**, (14), 2103670

The Authors

Pere L. Cabot defended his PhD in 1984 at the University of Barcelona (UB), Spain, and is full Professor of the Department of Materials Science and Physical Chemistry (Section of Physical Chemistry) of the UB since 2003. His current research topic is electrocatalysis in fuel cell and electrolysers, with special interest in polymetallic nanostructures and catalysts supports. He has participated in 50 competitive research projects, 31 contracts with companies and published 170 research papers, three international patents, 23 books and book chapters and about 200 meeting presentations and invited lectures. He has also received three awards from private companies, related to research, development and innovation.

Maria Victoria Martínez Huerta has held a Tenured Scientist position at the Institute of Catalysis and Petrochemistry (ICP) of the Spanish Council for Scientific Research (CSIC) since 2010 and is the head of the Electrocatalysis for Energy and the Environment Group. Her research activity is dedicated to the development of electrocatalysts that improve the activity and stability of electrodes in electrochemical devices for storage and conversion of clean energy, mainly in those applications that use hydrogen as an energy carrier such as fuel cells and electrolysers. She has participated in 39 competitive research projects and published 89 research papers (indexed in Web of Science™).

Francisco Alcaide holds a PhD in Chemistry (Physical Chemistry) from the University of Barcelona (2002). He has more than 25 years of experience in electrochemical technologies, especially in fuel cells and hydrogen. He has participated in or led about 50 national, European and international research, development and innovation projects and contracts with companies in technology transfer and innovation. He serves as independent expert and advisor for several national, international and European Commission public bodies. His research interests range from electrodics and electrocatalysis for clean energy and decarbonisation to batteries and water treatment. Alcaide currently works as Principal Investigator and Project manager at CIDETEC, Spain.